Topological quantum-phase coherence in full counting statistics of transport electrons with two-body interaction*

Guo Xiao-Fang(郭小芳)[a], Xue Hai-Bin(薛海斌)[b]†, and Liang Jiu-Qing(梁九卿)[a]‡

[a] *Institute of Theoretical Physics and Department of Physics, Shanxi University, Taiyuan* 030006, *China*
[b] *College of Physics and Optoelectronics, Taiyuan University of Technology, Taiyuan* 030024, *China*

(Received 20 January 2014; revised manuscript received 31 March 2014; published online 20 June 2014)

The full counting statistics of electron transport through two parallel quantum dots with antiparallel magnetic fluxes is investigated as a probe to detect the topological quantum-phase coherence (TQPC), which results in the characteristic oscillation of the zero-frequency cumulants including the shot noise and skewness. We show explicitly the phase transition of cumulant spectrum-patterns induced by the topology change of electron path-loops while the pattern period, which depends only on the topology (or Chern number), is robust against the variation of Coulomb interaction and interdot coupling strengths. Most importantly we report for the first time on a new type of TQPC, which is generated by the two-particle interaction and does not exist in the single-particle wave function interference. Moreover, the accurately quantized peaks of Fano-factor spectrum, which characterize the super- and sub-Poissonian shot noises, are of fundamental importance in technical applications similar to the superconducting quantum interference device.

Keywords: topological quantum-phase coherence, full counting statistics, two-body interaction

PACS: 73.23.–b, 03.65.Vf, 05.60.Gg, 71.10.Pm **DOI:** 10.1088/1674-1056/23/8/087308

1. Introduction

The full counting statistics (FCS) of electron transport through quantum dot (QD) systems have attracted considerable attention[1–25] because its FCS properties, i.e., the transport current high-order cumulants can allow one to identify the intrinsic properties of the QD system and access the information of electron correlation which cannot be obtained from the average current.[26,27] For example, the high-order cumulants can be used to detect the positions of the zeros of the generating function,[28] reveal the intrinsic multistability,[29] and extract the fractional charge of charge transfer through an impurity in a chiral Luttinger liquid,[30] and probe Majorana bound states in a nanowire.[31] A fundamental achievement in the field of FCS was reported recently that the third-order cumulant known as skewness of transport electron through a single tunnel junction can be measured experimentally.[32,33] Recently, theoretical studies have demonstrated that the high-order cumulants, e.g., the shot noise, the skewness, are more sensitive to the quantum coherence effect than the average current in different types of QD systems,[7,34–36] namely, the series DQD,[7] the side-coupled DQD,[25] the parallel DQD,[34] the Aharonov–Bohm interferometer with a quantum dot embedded in one of its two current paths,[35–37] a semiopen Kondo-correlated quantum dot.[38] In particular, the feasibility of extracting quantum coherence information from the current high-order cumulants has been predicted theoretically in a side-coupled double QD system.[25]

On the other hand, the quantum phase coherence of conduction electrons has become an active research field in the past decade with the measuring of magnetic-flux-dependent current through an Aharonov–Bohm (AB) interferometer.[39] The signature of coherent transport through the QD systems is characterized by the current oscillation with respect to the magnetic flux.[40] For an Aharonov–Bohm interferometer with single-level QDs embedded in the two arms, previous studies have demonstrated that the magnetic flux penetrating this Aharonov–Bohm ring have a great influence on the transport current noise properties.[11,12] For example, the finite-frequency current noise[11] and the super-Poissonian shot noise behavior[10] can be tunned by adjusting the external magnetic flux, and the values of the super-Poissonian shot noise and skewness will diverge when the magnetic flux approaches an integer multiple of the flux quantum.[12] The Fano line-shape in the DQD system can be possibly manipulated by tuning the coupling between two dots.[41] Recently Fano effects were explored in a system consisting of a QD and AB ring with both the magnetic and electrostatic manipulations.[42,43] Moreover modified Fano-resonances are observed in a Fano interferometer,[44,45] which are shown to be a result of the Coulomb-interaction.[46] In fact, the quantum coherence of conduction-electron through different channels is caused physically by the phase accumulation of spatial motion from the electrode to QD. Particularly, the AB phase coherence has a topological nature, namely, it does not de-

*Project supported by the National Natural Science Foundation of China (Grant Nos. 11075099. 11204203, and 11275118).
†Corresponding author. E-mail: xuehaibin@tyut.edu.cn
‡Corresponding author. E-mail: jqliang@sxu.edu.cn
© 2014 Chinese Physical Society and IOP Publishing Ltd

pend on the geometry of the paths and the coupling strengths but the topology of path loops. The topological nature of quantum coherence has not been explored yet on the FCS level for the mesoscopic coupled QDs system including two-body Coulomb interaction at finite temperatures. Additionally, the FCS of electron transport through a semiconductor quantum dot (QD) have been realized experimentally, especially the fifteen-order cumulants[14,15] and finite-frequency current statistics[19] can be extracted from the high-quality real-time single-electron measurements. This provides the opportunity to investigate the relationship between the AB phase coherence and the FCS of electron transport through a parallel-coupled double QDs system.

The quantum coherence of transmission through different channels is caused physically by the phase accumulation of spatial motion from the electrode to dot. Particularly the AB phase coherence has topological nature, that it does not depend on the geometry of the paths and the coupling strengths but the topology of path loops or more precisely the Chern numbers. The topological nature of quantum coherence has not yet been explored in the FCS for the mesoscopic transport system including two-body Coulomb interaction at finite temperatures. We, in this paper, consider a DQD threaded by a double magnetic flux line of parallel and antiparallel configurations (see Fig. 1) with a tunable interdot coupling to change the topology of transmission path loops. We show explicitly the topology-induced phase transition of the cumulant spectrum patterns. Most importantly a new type of topological quantum phase coherence (TQPC), which does not exist in the single-particle transport only at one time, is observed and successfully explained by the two-particle Coulomb interaction. The positions of characteristic resonance peaks in the Fano line-shape are accurately quantized and are shown to be robust against the magnitude variations of interdot coupling and Coulomb interaction, which however can manipulate the peak heights. Our observations may have practical applications in electronic devices.

2. Model and formalism

2.1. Statistical cumulants and related measurement quantities

The FCS is a fascinating theoretical approach, since it can yield simultaneously all cumulants of transport electrons and thus provide the information of transferred particle-number probability distribution $P(n,t)$ through the DQD system during a time interval t. The cumulant generation function (CGF)[47] is defined as

$$\mathrm{e}^{-F(\chi)} = \sum_n P(n,t)\,\mathrm{e}^{\mathrm{i}n\chi}, \tag{1}$$

where χ is the counting field and the exponent of the CGF, i.e., $F(\chi)$ plays a central role in our formalism. The cumulants of transport electrons can be obtained from the derivatives of $F(\chi)$ with respect to the counting field χ such that

$$C_k = -\left(-\mathrm{i}\frac{\partial}{\partial\chi}\right)^k F(\chi)|_{\chi=0.} \tag{2}$$

In the long-time limit, the first three cumulants are directly related to the measurement quantities of transport. The first-order cumulant C_1, which indicates the average number of transferred particles $\bar{n}$ and is actually the peak position of $P(n,t)$, gives rise to the average current defined by

$$\langle I\rangle = \frac{eC_1}{t}. \tag{3}$$

The zero-frequency shot noise is related to the second-order cumulant C_2 (i.e. the peak-width of the distribution $P(n,t)$) such as

$$S = \frac{2\mathrm{e}^2C_2}{t} = \frac{2\mathrm{e}^2(\overline{n^2}-\bar{n}^2)}{t}. \tag{4}$$

Finally the third-order cumulant $C_3 = \overline{(n-\bar{n})^3}$ characterizes the skewness of $P(n,t)$. The normalized Fano factor and skewness are defined respectively by

$$F_\mathrm{a} = \frac{C_2}{C_1}, \quad S_\mathrm{k} = \frac{C_3}{C_1}. \tag{5}$$

Fano factor F_a represents the amplitude of current fluctuations with $F_\mathrm{a} > 1$ indicating a super-Poissonian fluctuation, and $F_\mathrm{a} < 1$ a sub-Poisson process.

2.2. Model Hamiltonian and topological quantum phases

We consider in the present paper a system of two parallel single-level QDs weakly connected to two metallic electrodes, which is described by the Hamiltonian

$$H = H_\mathrm{dot} + H_\mathrm{leads} + H_\mathrm{T}. \tag{6}$$

with QD part denoted by

$$H_\mathrm{dot} = \varepsilon_1 d_1^\dagger d_1 + \varepsilon_2 d_2^\dagger d_2 - J(d_1^\dagger d_2 + d_2^\dagger d_1) + U d_1^\dagger d_1 d_2^\dagger d_2, \tag{7}$$

where $d_i^\dagger$ (d_i) is the creation (annihilation) operator of an electron in the QD-i ($i = 1,2$) and ε_i is the bare energy level of electron in the same QD. J is tunable coupling constant between two dots and U denotes the Coulomb interaction whenever two electrons are respectively and simultaneously populated in the QD-1 and QD-2. The Hamiltonian of electrodes is

$$H_\mathrm{leads} = \sum_{\alpha k} \varepsilon_{\alpha k} a_{\alpha k}^\dagger a_{\alpha k}, \tag{8}$$

with $a_{\alpha k}^\dagger$ ($a_{\alpha k}$) being the creation (annihilation) of an electron with energy $\varepsilon_{\alpha k}$ and momentum k in the electrode-α ($\alpha =$ L,R). Two magnetic flux-lines of $\Phi_1 = \zeta_1\Phi_0$ and $\Phi_2 = \zeta_2\Phi_0$ are perpendicular to the plan of DQD-electrodes as shown in Fig. 1, where $\Phi_0 = ch/e$ is the quantum unit of magnetic flux

and thus ζ_1, ζ_2 are dimensionless flux numbers respectively. The existence of gauge potential (vector potential) of the magnetic fluxes leads to topological phases on the wave functions of electron transferred between dots and electrodes and the transmission Hamiltonian becomes

$$H_{\rm T} = \sum_{\alpha,k,i} (t_{\alpha ik} F_{\alpha i} a^{\dagger}_{\alpha ki} d_i + {\rm h.c.}). \tag{9}$$

The topological phases from electrode-α to QD-i are given by

$$\begin{aligned} F_{\rm L1} &= {\rm e}^{{\rm i}\pi\zeta_1}, \quad F_{\rm L2} = {\rm e}^{-{\rm i}\pi\zeta_1}, \\ F_{\rm R1} &= {\rm e}^{-{\rm i}\pi\zeta_2}, \quad F_{\rm R2} = {\rm e}^{{\rm i}\pi\zeta_2}, \end{aligned} \tag{10}$$

where we have assumed that the flux number ζ_i is positive when the magnetic field is pointed into the QD-electrode plan as the left-hand flux shows in Fig. 1. $t_{\alpha ik}$ is the coupling constant between QD-α and electrode-i. We define the reservoir annihilation-operators of the left and right electrodes such that

$$\begin{aligned} A_{{\rm L}i} &= \sum_{\rm k} t^{*}_{{\rm L}ik} F^{\dagger}_{{\rm L}i} a_{\alpha ki}, \quad A_{{\rm R}i} = \sum_{\rm k} t^{*}_{{\rm R}ik} F^{\dagger}_{{\rm R}i} a_{\alpha ki}, \\ A_i &= A_{{\rm L}i} + A_{{\rm R}i}. \end{aligned} \tag{11}$$

Although the case of two arbitrary fluxes can be formulated, we are interested in the parallel ($\zeta_1 = \zeta_2 = \zeta$) and antiparallel ($\zeta_1 = -\zeta_2 = \varsigma$) configurations with equal amount of fluxes.

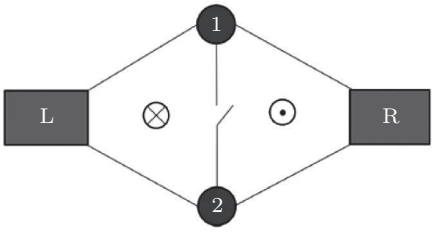


Fig. 1. Schematic diagram of the double quantum dots with two antiparallel fluxes and tunable interdot coupling to change the topology of carrier path loop.

The tunable interdot coupling plays a crucial role in our investigation. When the coupling is switched off ($J = 0$) one has a one-loop topology and the system reduces to a double-line AB interferometer for the parallel configuration, while the TQPC does not exist at all for the antiparallel configuration in the case of single-particle transport since the total flux is zero. We are particularly interested in the antiparallel configuration for the topology-change-induced coherence and the new type of TQPC generated by the two-particle occupation.

In the Coulomb-blockade regime such that only one-electron at most can be populated in each dot at one time, four occupation states are obtained as[21]

$$\begin{aligned} |\Psi_0\rangle &= |0,0\rangle, \\ |\Psi_1\rangle^{-} &= a_- |1,0\rangle + b_- |0,1\rangle, \\ |\Psi_1\rangle^{+} &= a_+ |1,0\rangle + b_+ |0,1\rangle, \end{aligned}$$

$$|\Psi_2\rangle = |1,1\rangle, \tag{12}$$

with the coefficients given by

$$\begin{aligned} a_{\pm} &= \frac{\mp J}{\sqrt{J^2 + (\varepsilon_1 - \varepsilon_{\pm})^2}}, \\ b_{\pm} &= \frac{\pm(\varepsilon_{\pm} - \varepsilon_1)}{\sqrt{J^2 + (\varepsilon_1 - \varepsilon_{\pm})^2}}. \end{aligned} \tag{13}$$

Energy eigenvalues corresponding to these states are seen to be

$$\begin{aligned} \varepsilon_0 &= 0, \\ \varepsilon_- &= \frac{\varepsilon_1 + \varepsilon_2 - \sqrt{(\varepsilon_1 - \varepsilon_2)^2 + 4J^2}}{2}, \\ \varepsilon_+ &= \frac{\varepsilon_1 + \varepsilon_2 + \sqrt{(\varepsilon_1 - \varepsilon_2)^2 + 4J^2}}{2}, \\ \varepsilon_{11} &= \varepsilon_1 + \varepsilon_2 + U. \end{aligned} \tag{14}$$

In order to see the effect of Coulomb interaction on the TQPC we also present the result of single-particle transitions as comparison. This case can be considered as the ultrastrong Coulomb-blockade regime such that only one-electron at most can be populated in the whole DQD at one time and thus the occupation probability of the two-electron state $|\Psi_2\rangle$ vanishes.

2.3. Method of quantum master equation

The particle transitions are well described by quantum master equation of a reduced density matrix spanned by the eigenstates of coupled single-level DQD. Regarding the tunneling Hamiltonian $\widehat{H}_{\rm T}$ as a perturbation, the second-order cumulant expansion under Born and Markov approximations leads to the following particle-number-resolved quantum master equation for the reduced density matrix $\rho^{(n)}(t)$[9,48,49]

$$\frac{\partial \rho^{(n)}(t)}{\partial t} = -{\rm i}\mathcal{L}(t)\rho^{(n)}(t) - \frac{1}{2} R\rho^{(n)}(t), \tag{15}$$

where

$$\begin{aligned} R\rho^{(n)}(t) = \sum_{\substack{\alpha={\rm L,R} \\ ij=1,2}} \{ & \rho^{(n)}(t) D^{(+)}_{\alpha,i} d^{\dagger}_j + d^{\dagger}_j D^{(-)}_{\alpha,i} \rho^{(n)}(t) \\ & - D^{(-)}_{{\rm L},i} \rho^{(n)}(t) d^{\dagger}_j - D^{(-)}_{{\rm R},i} \rho^{(n-1)}(t) d^{\dagger}_j \\ & - d^{\dagger}_j \rho^{(n)}(t) D^{(+)}_{{\rm L},i} - d^{\dagger}_j \rho^{(n+1)}(t) D^{(+)}_{{\rm R},i} + {\rm h.c.} \} \end{aligned} \tag{16}$$

with

$$D^{(\pm)}_{\alpha,i} = \sum_j C^{(\pm)}_{\alpha ij}(\pm\mathcal{L}) d_j, \tag{17}$$

in which the spectral functions are defined in terms of the Fourier transform of the reservoir correlation functions, i.e.,

$$\begin{aligned} C^{(+)}_{\alpha ij}(\mathcal{L}) &= \int {\rm d}\tau C^{(+)}_{\alpha ji}(-\tau) \exp[-{\rm i}\mathcal{L}\tau], \\ C^{(-)}_{\alpha ij}(-\mathcal{L}) &= \int {\rm d}\tau C^{(-)}_{\alpha ij}(\tau) \exp[-{\rm i}\mathcal{L}\tau], \end{aligned} \tag{18}$$

with $t-t'=\tau$. The reservoir correlation functions read

$$C^{(+)}_{\alpha ij}(t-t')=\left\langle A^{\dagger}_{\alpha i}(t)A_{\alpha j}(t')\right\rangle, \tag{19}$$

and

$$C^{(-)}_{\alpha ij}(t-t')=\left\langle A_{\alpha i}(t)A^{\dagger}_{\alpha j}(t')\right\rangle. \tag{20}$$

Here $\langle\cdots\rangle$ stands for $\mathrm{Tr}_B[\ldots\rho^{(0)}_B]$, with the usual meaning of thermal average. The Liouvillian super-operator $\mathcal{L}$ is defined as the commutation relation

$$\mathcal{L}(\cdots)=[H,(\cdots)]. \tag{21}$$

Throughout this paper, we set $e=\hbar=1$. The reduced density matrix $\rho^{(n)}(t)$ is related to the electron numbers arriving at the right electrode up to time t. We introduce the notation

$$\begin{aligned} D^{(+)}_{\alpha} &= \sum_i D^{(+)}_{\alpha i}=\sum_{ij} C^{(+)}_{\alpha ij}(+\mathcal{L})d_j \\ &= \sum_j \Gamma_{\alpha} n^{(+)}_{\alpha}(-\mathcal{L})d_j, \end{aligned} \tag{22}$$

where

$$\Gamma_{\alpha=\mathrm{L,R}}=2\pi g_{\alpha=\mathrm{L,R}} t_{\mathrm{L}i,\mathrm{R}i}\Gamma_{\mathrm{L}i,\mathrm{R}i}t^{*}_{\mathrm{L}j,\mathrm{R}j}\Gamma^{\dagger}_{\mathrm{L}j,\mathrm{R}j} \tag{23}$$

is the coupling strength to the electrode-α and

$$n^{(+)}_{\alpha}(\varepsilon_{\alpha k})=\mathrm{Tr}_B[a^{\dagger}_{\alpha k}a_{\alpha k}\rho^{(0)}_B], \tag{24}$$

$g_{\alpha=\mathrm{L,R}}$ denotes the density of states in the electrodes. An asymmetry parameter $\theta=|\Gamma_{\mathrm{R}}|/|\Gamma_{\mathrm{L}}|$ is introduced to describe the imbalance between the transitions from the DQD to the right and left electrodes, which is useful in the manipulation of resonance peak-heights of Fano line-shape generated by the TQPC. Similarly we have

$$\begin{aligned} D^{(-)}_{\alpha} &= \sum_i D^{(-)}_{\alpha i}=\sum_{ij} C^{(-)}_{\alpha ij}(-\mathcal{L})d_j \\ &= \sum_j \Gamma^{*}_{\alpha} n^{(-)}_{\alpha}(-\mathcal{L})d_j, \end{aligned} \tag{25}$$

where

$$n^{(-)}_{\alpha}(\varepsilon_{\alpha k})=\mathrm{Tr}_B[a_{\alpha k}a^{\dagger}_{\alpha k}\rho^{(0)}_B]. \tag{26}$$

We moreover assume the wide band approximation that $n^{(+)}_{\alpha}=f_{\alpha}$, $n^{(-)}_{\alpha}=1-f_{\alpha}$, where f_{α} is the Femi distribution function of the electrode-α. In order to calculate the CGF, one can define a column matrix

$$G(\chi,t)=\sum_n \rho^{(n)}(t)\,\mathrm{e}^{\mathrm{i}n\chi}. \tag{27}$$

Evidently, the CGF can be evaluated as

$$\mathrm{e}^{-F(\chi)}=\mathrm{Tr}[G(\chi,t)], \tag{28}$$

where the trace is over the eigenstates of the considered DQD system. Since equation (15) has the following form

$$\dot{\rho}^{(n)}=\boldsymbol{A}\rho^{(n)}+\boldsymbol{C}\rho^{(n+1)}+\boldsymbol{D}\rho^{(n-1)}. \tag{29}$$

The column matrix $G(\chi,t)$ satisfies the equation

$$\dot{G}=\boldsymbol{L}_{\chi}G \tag{30}$$

with the matrix operator defined by

$$\boldsymbol{L}_{\chi}=\boldsymbol{A}+\mathrm{e}^{-\mathrm{i}\chi}\boldsymbol{C}+\mathrm{e}^{\mathrm{i}\chi}\boldsymbol{D}. \tag{31}$$

where $\boldsymbol{A}$, $\boldsymbol{C}$, and $\boldsymbol{D}$ are three square matrices. In the low frequency limit, the counting time (i.e., the time of measurement) is much longer than the time of electron tunneling through the DQD system. In this case, the exponent of the CGF $F(\chi)$ can be expressed as[7–9,47,50–52]

$$F(\chi)=-\lambda_1(\chi)t, \tag{32}$$

where $\lambda_1(\chi)$ is the eigenvalue of operator $\boldsymbol{L}_{\chi}$, which goes to zero when $\chi\longrightarrow 0$. According to the definition of cumulants one can express $\lambda_1(\chi)$ as

$$\lambda_1(\chi)=\frac{1}{t}\sum_{\mathrm{k}=1}^{\infty}C_{\mathrm{k}}\frac{(\mathrm{i}\chi)^k}{k!}. \tag{33}$$

The specific form of $\boldsymbol{L}_{\chi}$ can be obtained by performing a discrete Fourier transformation to the matrix elements of Eq. (15). Inserting Eq. (33) into the secular equation

$$|\boldsymbol{L}_{\chi}-\lambda_1(\chi)I|=0 \tag{34}$$

and expanding this determinant in series of $(\mathrm{i}\chi)^k$, one can calculate C_{k}/t by setting the coefficient of $(\mathrm{i}\chi)^k$ equal to be zero. The numerical results of the cumulants are shown in the following section with the particular attention on the TQPC.

3. Full counting statistics analysis

3.1. Quantum phase-interference and topology-change induced oscillation

The complete information about quantum coherence can be extracted from all cumulants of the number distribution $P(n,t)$ of transferred carriers, which are indeed useful quantities to characterize transport mechanism. The magnetic flux-dependence of average current defined by Eq. (2) in relation with the first-order cumulant C_1, which as a matter of fact is the peak position of the transferred electron-number probability $P(n,t)$, is plotted in Fig. 2 for both parallel (a) and antiparallel (b) configurations. To see the typical AB interference we in Fig. 2 consider the ultrastrong Coulomb-blockade regime with the single-particle occupation in the whole DQD only. When the interdot coupling is switched off ($J=0$) the system is a one-loop interferometer with a double-flux (2ζ) for the parallel configuration. The current displays a single-mode oscillation of period $1/2$ (in the unit of Φ_0) seen from

the solid line of Fig. 2(a), while there is no topological phase interference at all for the antiparallel configuration [Fig. 2(b) solid line (black)] as it should be, since the total flux embraced by the loop is zero. When the interdot coupling is turned on the interference patterns for the parallel configuration are essentially the same since the additional interdot paths give rise to no phase changes [Fig. 2(a) dotted (blue) and dashed (red) lines] in this case (the quantum phases accumulated from the gauge potentials of two fluxes cancel each other). While, on the other hand the TQPC emerges for the antiparallel configuration due to the interdot paths showing a topology-induced phase transition [Fig. 2(b) dashed and dotted lines for $0.5\,J=1$ respectively]. The oscillation period in this case is 1 because each loop embraces only one flux of value ζ. The variation of coupling constant J can only change the amplitude of oscillation but not the period, which is the characteristic of the TQPC. All the figures in this paper are plotted at a finite temperature $\beta = 1/k_{\rm B}T = 0.15$, energy eigenvalues of the two dots $\varepsilon_2 = -\varepsilon_1 = 0.5$, and the chemical potentials of electrodes $\mu_{\rm L} = -\mu_{\rm R} = 20$ (the bias voltage is $V = \mu_{\rm L} - \mu_{\rm R} = 40$) respectively in the energy unit of meV throughout the paper which corresponds to a typical experimental situation.[53]

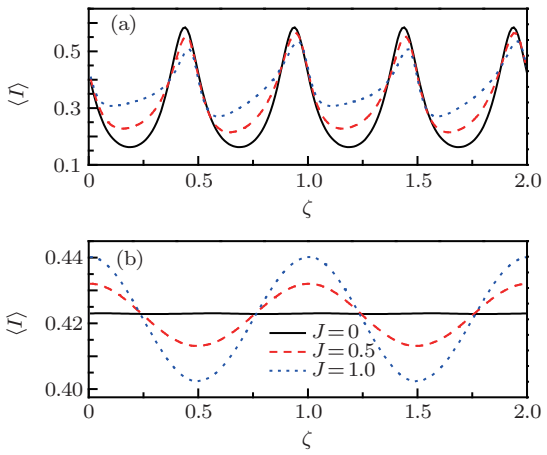


Fig. 2. (color online) The average current versus magnetic flux in ultrastrong Coulomb-blockade regime with one electron occupation only for parallel (a) and antiparallel (b) configurations with $J = 0$, 0.5, 1 respectively and $\theta = 1$.

3.2. Quantum phase-interference generated by Coulomb interaction

What we considered in Fig. 2 is the typical single-particle quantum phase coherence, i.e., the well-known AB effect and is realized in the ultrastrong Coulomb-blockade regime. The AB interference disappears when the interdot coupling is switched off ($J = 0$) seen from Fig. 2(b) (solid line) for the antiparallel configuration. Now we turn to the usual Coulomb blockade regime with a finite value of Coulomb-interation strength U, which allows the non-zero occupation probability of the two-particle state $|\Psi_2\rangle$. It is certainly of interest to see the effect of two-particle interaction, which has not yet been explored to our knowledge. To this end we present, in Figs. 3, 4, and 5, the same current plots for the Coulomb interaction constants $U = 5$, 20, and 40 respectively. For the parallel configuration the interference patterns in Figs. 3, 5(a) with $U = 5, 40$ are essentially not changed compared with the single-particle case, since the effect of two-electron occupation in these two cases is small and the transition process is still dominated by the single-particle transport. For $U = 20$ the oscillation period is essentially $1/2$ for $J = 0.5$, 1 [Fig. 4(a), dashed and dotted lines], while the pattern shape has an apparent variation with alternate lower and higher peaks for $J = 0$ [Fig. 4(a) solid line] caused by the superposition of two-particle and single-particle transitions. For the antiparallel configuration we observed a peculiar quantum interference oscillation, that when the interdot coupling is switched off (i.e. no particle transition between two dots) the interference oscillation still exists different from the single-particle transition [Fig. 2(b) (solid line)]. The oscillation period is $1/2$ and the amplitudes vary along with the Coulomb-interaction constant U for the fixed bias voltage seen from Figs. 3, 4, 5(b) (solid lines). This new interference oscillation is obviously generated by the two-particle interaction and can be understood from the wave-function overlap of two transported (identical) particles from the electrode to the DQD, which results in an interference factor $(1 - \delta\cos 4\pi\zeta)$ giving rise to the oscillation of period $1/2$ with the wave troughs located at integer and half-integer. The parameter δ is proportional to the Coulomb-interaction constant U and the occupation probability of two-particle state $|\Psi_2\rangle$. The oscillation amplitude for $U = 5$ [Fig. 3(b) solid line] is a small value about 0.004 (electron charge per unit time) and increases to the highest value 0.02 [Fig. 4(b)] when the Coulomb-interaction constant becomes 20, i.e. $1/2$ bias-voltage V. Then, the oscillation amplitude decreases with U above the critical value and becomes negligibly small at $U = 40$. This is because the high Coulomb-interaction energy suppresses the occupation probability of two-particle state $|\Psi_2\rangle$. Above the value $U = V$ it is

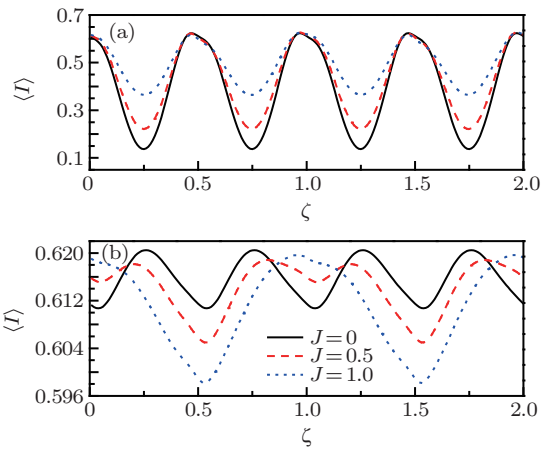


Fig. 3. (color online) The average current versus magnetic flux: (a) parallel (b) antiparallel configurations for $U = 5$, and $\theta = 1$.

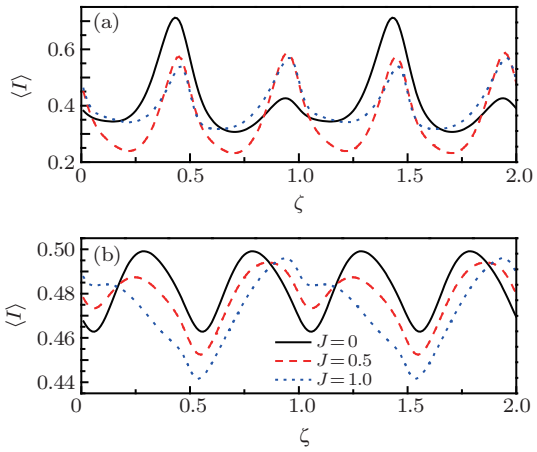


Fig. 4. (color online) The average current versus magnetic flux: (a) parallel (b) antiparallel configurations for $U = 20$, and $\theta = 1$.

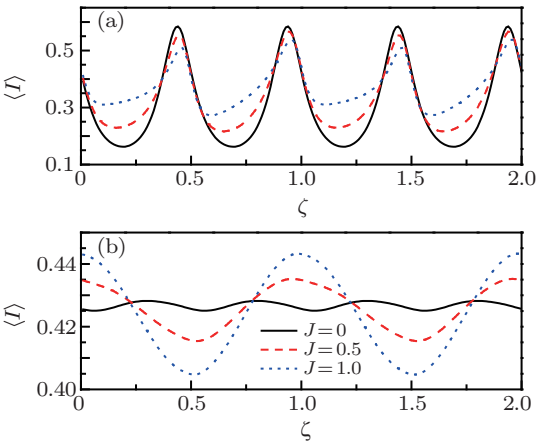


Fig. 5. (color online) The average current versus magnetic flux: (a) parallel (b) antiparallel configurations for $U = 40$, and $\theta = 1$.

essentially the ultrastrong Coulomb-blockade regime with the single-electron occupation only in the DQD seen from the similarity between Figs. 2(b) and 5(b). When the interdot coupling is switched on with nonvanishing J, the interdot tunnel path of the single-particle occupation gives rise to the interference oscillation of period 1 with higher amplitudes depending on the value of J [see Figs. 3, 4, 5(b) dotted and dashed lines]. The interference patterns with the interdot coupling obviously come from the superposition of two-particle and single-particle transitions.

3.3. Shot noise and skewness as a probe to detect the topological phase coherence

The shot noise (or Fano factor F_a) and skewness S_k in relation with the zero-frequency cumulants C_2 and C_3 are shown to be the quantities most sensitive to the TQPC and Coulomb interaction. The measurements of shot noise can yield more information about the microscopic mechanism of transport. We now demonstrate the effect of TQPC on the Fano factor F_a and skewness S_k, which in turn can serve as probes to detect the TQPC. Figure 6 displays the numerical results of F_a (upper panels) and S_k (lower panels) for $U = 5$ (a), 20 (b), and 40 (c) respectively. When the interdot coupling is switched off ($J = 0$, solid line in Fig. 6) the wave-trains of period $1/2$ for both F_a and S_k are generated by the Coulomb interaction of two-electron state occupation. The wave-trains heights of F_a and S_k are respectively 0.005 and 0.01 for $U = 5$.

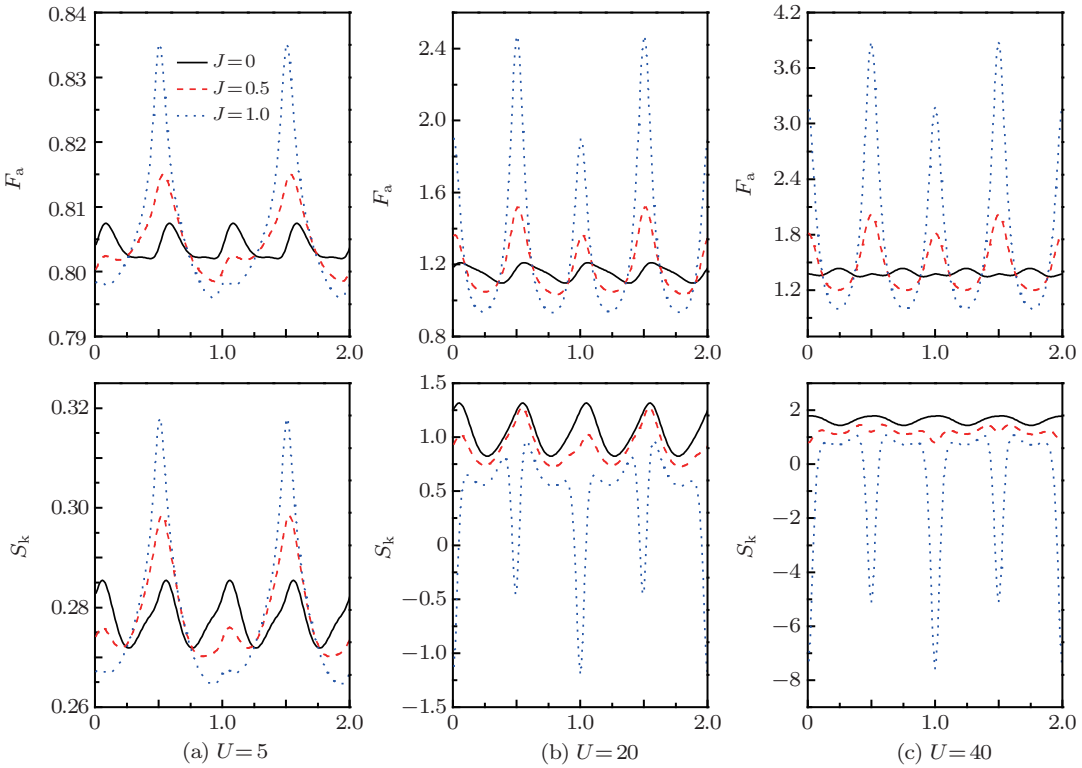


Fig. 6. (color online) F_a (upper panels) and S_k (lower panels) spectrums with respect to the flux for the antiparallel configuration with $\theta = 1$. (a) $U = 5$, (b) $U = 20$, (c) $U = 40$.

The heights increase with U up to highest values 0.1 and 0.5 when U reaches the critical value $V/2$. Then the heights decrease with increasing U due to the suppression of occupation probability of two-electron state $|\Psi_2\rangle$. The U-dependence behavior is the same as the oscillation amplitude of average current, while the period of wave-trains indicating the topological nature is independent of the U variation. When interdot coupling is turned on the tunnel paths between two dots give rise to the interference oscillation of period 1. The F_a and S_k oscillation patterns (dotted and dashed lines in Fig. 6) are simply the superposition of two-mode oscillations of periods 1 and $1/2$. The high peaks of F_a spectrums and dips of S_k (for $U = 20$, 40) are quantized exactly with position spacing $\Phi_0/2$. This new observation can be developed to a quantum interferometer to measure ultraweak magnetic field similar to the superconducting quantum interference device.

3.4. Manipulation of resonance peaks, super- and sub-Poissonian noises

We have demonstrated that the period of topological phase oscillation is robust against the variation of interdot coupling and the Coulomb interaction as well. However the magnitudes of correlation functions are sensitive to the system parameters especially the asymmetry parameter θ. The resonance peak heights of F_a and S_k at the integer number of flux (or integer Chern number) as a function of the asymmetry parameter θ are displayed in Fig. 7 for the ultrastrong (single-electron occupation only) [(a), (b)] and finite (with double-electron occupation) [(c), (d)] Coulomb interactions respectively with different interdot couplings. It is of interest to note that super-Poissonian noise with $F_a > 1$ is found in the ultrastrong Coulomb-blockade regime with single-electron occupation only [panel (a)] and F_a increases with J since the interdot coupling opens additional transition channels. The correlation functions are essentially sub-Poissonian for two-particle occupation in a finite Coulomb-interaction [panel (c)] in agreement with the observation that the sub-Poissonian shot noise of current fluctuation resulted usually from the Fermi–Dirac statistics when the many-body Coulomb interaction is considered.[9] The reason why F_a and S_k do not change essentially with the variation of J is that the interdot channel is blocked in the double-occupation case. F_a has minimum value at the symmetric dot-electrode transition with $\theta = 1$ and increases with deviation from the symmetric case, since the asymmetry may lead to the reflection of transport electrons favoring quantum fluctuation of current. We mainly show here that the resonance peak-heights of F_a and S_k can be manipulated by the asymmetry parameter θ.

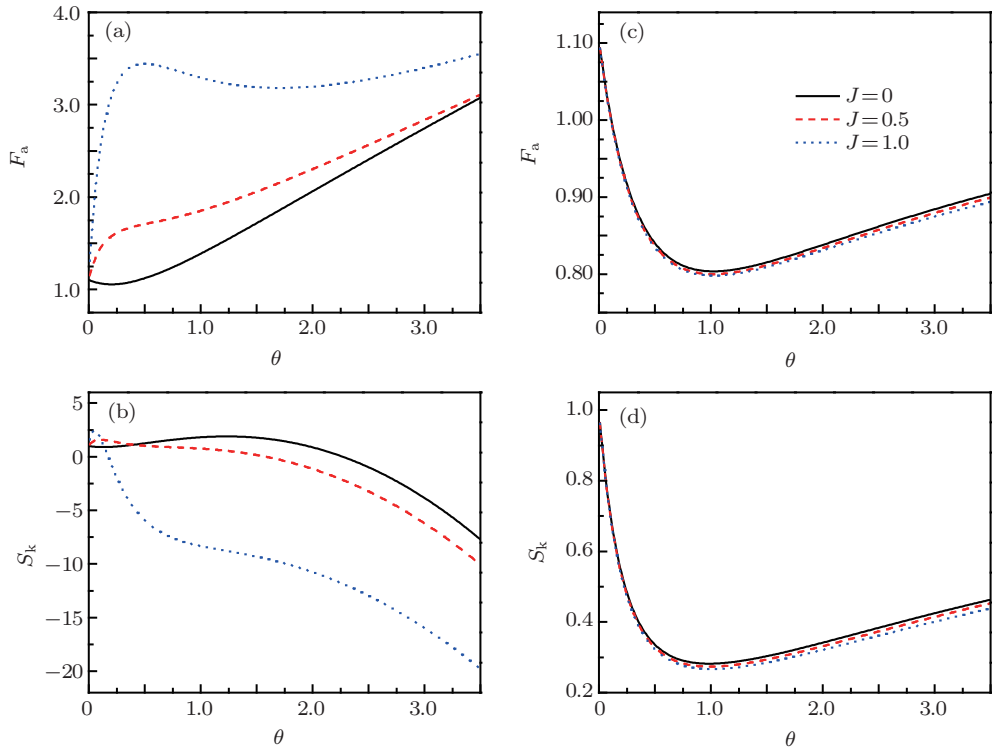


Fig. 7. (color online) F_a [panels (a) and (c)] and S_k [panels (b) and (d)] versus θ for zero (integer) magnetic flux in ultrastrong Coulomb blockade regime [panels (a) and (b)] and $U = 5.0$ with double-eletron occupation [panels (c) and (d)].

4. Conclusion and discussion

In summary, the TQPC has been studied in the FCS of transport electrons through a DQD system with two-body interaction at finite temperature. Indeed the cumulants in FCS are so sensitive to the TQPC and thus can serve as a probe to detect the effect. For the antiparallel configuration of mag-

netic fluxes we show explicitly the topology change-induced oscillation of the first-order cumulant (in relation to transport current). The oscillation period characterizing the TQPC is robust against the amplitude variation of the interdot coupling and the Coulomb interaction as well. The accurately quantized resonance peaks (or dips) of the second- and third-order cumulants are localized at the integer or half-integer number of fluxes in the quantum unit Φ_0. Thus the mesoscopic system can be used to measure the magnetic field embraced by the two arms of the DQD similar to the superconducting quantum interference device. It is remarkable to observe a new type of the TQPC, which is generated by the Coulomb interaction of two-electron occupation in the DQD and does not exist for the single-particle occupation only. Finally, we show the manipulation of resonance peak heights by the interdot and dot-electrode couplings.

References

[1] Lu W, Ji Z, Pfeier L, West K W and Rimberg A J 2003 *Nature* **423** 422
[2] Fujisawa T, Hayashi T, Hirayama Y, Cheong H D and Jeong Y H 2004 *Appl. Phys. Lett.* **84** 2343
[3] Gustavsson S, Leturcq R, Simovič B, Schleser R, Ihn T, Studerus P, Ensslin K, Driscoll D C and Gossard A C 2006 *Phys. Rev. Lett.* **96** 076605
[4] Fujisawa T, Hayashi T, Tomita R and Hirayama Y 2006 *Science* **312** 1634
[5] Djuric I, Dong B and Cui H L 2005 *Appl. Phys. Lett.* **87** 032105
[6] Aghassi J, Thielmann A, Hettler M H and Schön G 2006 *Phys. Rev. B* **73** 195323
[7] Kießlich G, Samuelsson P, Wacker A and Schöll E 2006 *Phys. Rev. B* **73** 033312
[8] Groth C W, Michaelis B and Beenakker C W J 2006 *Phys. Rev. B* **74** 125315
[9] Wang S K, Jiao H, Li F and Li X Q 2007 *Phys. Rev. B* **73** 125416
[10] Qin L and Guo Y 2008 *J. Phys.: Condens. Matter* **20** 365206
[11] Dong B, Lei X L and Horing N J M 2008 *J. Appl. Phys.* **104** 033532
[12] Urban D and König J 2009 *Phys. Rev. B* **79** 165319
[13] Lindebaum S, Urban D and König J 2009 *Phys. Rev. B* **79** 245303
[14] Flindt C, Fricke C, Hohls F, Novotný T, Netočný K, Brandes T and Haug R J 2009 *Proc. Natl. Acad. Sci. USA* **106** 10116
[15] Fricke C, Hohls F, Sethubalasubramanian N, Fricke L and Haug R J 2010 *Appl. Phys. Lett.* **96** 202103
[16] Luo J Y, Jiao H J, Shen Y, Cen G, He X L and Wang C 2011 *J. Phys.: Condens. Matter* **23**
[17] Luo J Y, Shen Y, He X L, Li X Q and Yan Y J 2011 *Phys. Lett. A* **376** 59
[18] Jin J S, Li X Q, Luo M and Yan Y J 2011 *J. Appl. Phys.* **109** 053704
[19] Ubbelohde N, Fricke C, Flindt C, Hohls F and Haug R J 2012 *Nat. Commun.* **3** 612
[20] Choi T, Ihn T, Schön S and Ensslin K 2012 *Appl. Phys. Lett.* **100** 072110
[21] Xue H B, Zhang Z X and Fei H M 2012 *Eur. Phys. J. B* **85** 336
[22] Komijani Y, Choi T, Nichele F, Ensslin K, Ihn T, Reuter D and Wieck A D 2013 *Phys. Rev. B* **88** 035417
[23] Fricke L, Wulf M, Kaestner B, Kashcheyevs V, Timoshenko J, Nazarov P, Hohls F, Mirovsky P, Mackrodt B, Dolata R, Weimann T, Pierz K and Schumacher H W 2013 *Phys. Rev. Lett.* **110** 126803
[24] Zhang H W, Xue H B and Nie Y H 2013 *AIP Advances* **3** 102116
[25] Xue H B 2013 *Annals of Physics* **339** 208
[26] Blanter Y M and Bütiker M 2000 *Phys. Rep.* **336** 1
[27] Nazarov Y V 2003 *Quantum Noise in Mesoscopic Physics* (Dordrecht: Kluwer) pp. 1–20
[28] Kambly D, Flindt C and Büttiker M 2011 *Phys. Rev. B* **83** 075432
[29] Schaller G, Kießlich G and Brandes T 2010 *Phys. Rev. B* **81** 205305
[30] Komnik A and Saleur H 2006 *Phys. Rev. Lett.* **96** 216406
[31] Li Z Z and You J Q 2013 arXiv: **1311** 4724
[32] Reulet B, Senzier J and Prober D E 2003 *Phys. Rev. Lett.* **91** 196601
[33] Bomze Y, Gershon G, Shovkun D, Levitov L S and Reznikov M 2005 *Phys. Rev. Lett.* **95** 176601
[34] Welack S, Esposito M, Harbola U and Mukamel S 2008 *Phys. Rev. B* **77** 195315
[35] Fang T F, Wang S J and Zuo W 2007 *Phys. Rev. B* **76** 205312
[36] Zhang Q Y, Wang B G and Xing D Y 2010 *Chin. Phys. Lett.* **27** 097401
[37] Li Z J 2005 *Chin. Phys.* **14** 2100
[38] Fang T F, Zuo W and Chen J Y 2008 *Phys. Rev. B* **77** 125136
[39] Yu H L, Wang Z G and Peng J 2009 *Chin. Phys. B* **18** 5485
[40] Holleitner A W, Decker C R, Qin H, Eberl K and Blick R H 2001 *Phys. Rev. Lett.* **87** 256802
[41] Schuster R, Buks E, Heiblum M, Mahalu D, Umansky V and Shtrikman H 1997 *Nature* **385** 417
[42] Kobayashi K, Aikawa H, Katsumoto S and Iye Y 2002 *Phys. Rev. Lett.* **88** 256806
[43] Kobayashi K, Aikawa H, Katsumoto S and Iye Y 2003 *Phys. Rev. B* **68** 235304
[44] Johnson A C, Marcus C M, Hanson M P and Gossard A C 2004 *Phys. Rev. Lett.* **93** 106803
[45] Chen X W, Chen B J, Shi Z G and Song K H 2009 *Acta Phys. Sin.* **58** 2713 (in Chinese)
[46] Lu H Z, Lü R and Zhu B F 2005 *Phys. Rev. B* **71** 235320
[47] Bagrets D A and Nazarov Yu V 2003 *Phys. Rev. B* **67** 085316
[48] Li X Q, Cui P and Yan Y J 2005 *Phys. Rev. Lett.* **94** 066803
[49] Li X Q, Luo J, Yang Y G, Cui P and Yan Y J 2005 *Phys. Rev. B* **71** 205304
[50] Flindt C, Novotný T and Jauho A P 2005 *Europhys. Lett.* **69** 475
[51] Flindt C, Novotný T, Braggio A, Sassetti M and Jauho A P 2008 *Phys. Rev. Lett.* **100** 150601
[52] Flindt C, Novotný T, Braggio A and Jauho A P 2010 *Phys. Rev. B* **82** 155407
[53] Elzerman J M, Hanson R, Willems van Beveren L H, Witkamp B, Vandersypen L M K and Kouwenhoven L P 2004 *Nature* **430** 431